High Resolution Dispersed Reference Interferometry

James Williamson, Haydn Martin, Xiangqian Jiang
University of Huddersfield, Queensgate, Huddersfield, HD1 3DH, United Kingdom

Dispersed reference interferometry (DRI) is a single point measurement technique with potential for use in applications such as absolute displacement, surface topography and film thickness measurement. A dispersed reference interferometer using a short coherence near infrared light source is described with chromatic dispersion in the reference arm introduced by a pair of matched transmission gratings. By tracking the point of symmetry of the produced interferogram, absolute position measurement may be performed. A previously demonstrated method (Martin 2013) to provide single point measurements is described and further simulated and experimental evidence is provided to demonstrate the potential capability of DRI to provide higher vertical resolution relative measurement while maintaining range.

Keywords: Optical interferometry, surface measurement, optical metrology, profile measurement.

1. Introduction

Dispersed reference interferometry (DRI) is a novel single point measurement technique with potential applications in ultra and high precision manufacturing which include surface profilometry and film measurement. The principle behind DRI is the introduction of chromatic dispersion in the reference arm of a Michelson type interferometer. The technique has previously been demonstrated (Martin 2013) to be capable of a vertical range competitive with existing commercial alternatives but shows potential to provide metrology solutions at a lower price and in difficult to measure locations due to the proposed use of inexpensive, commercially available common path fibre linked probes. These miniature probes along with the proposed novel configuration will lead to lower manufacturing costs of high precision components, reducing waste and measurement time by facilitating a flexible, on-machine solution. The principle is adapted from a dispersed reference interferometer demonstrated by Pavlíček and Häusler (Häusler 2005), using diffraction gratings instead of dispersive index fibre in order to eliminate non-common path errors introduced by long lengths of fibre.

In this paper we report new signal processing methods to extract high resolution data from DRI without alterations to the experimental bulk optics apparatus. This measurement data has the potential, when used in conjunction with the previous method, to provide the desired high dynamic range measurement results.

2. Operational Principles

The experimental apparatus is a bulk optics setup comprised of a Michelson interferometer with a chromatically dispersed reference arm, a schematic of which is shown in Figure 1. A source light (S) is split by a beam splitter (BS) to form the two arms of the interferometer. In the measurement arm, a mirror (M1) reflects the incident light back to the beam splitter. In the reference arm, a pair of matched transmission gratings (G1, G2) introduce chromatic dispersion to the source light. The first grating (G1) acts to separate the source wavelengths spatially while the second grating (G2) re-collimates the beam. The reference mirror (M2) reflects the beam back through both gratings, effectively doubling the dispersion. The effect of using these gratings is that the longer source wavelengths are dispersed by a higher angle, θ, and so travel further than the shorter wavelengths.

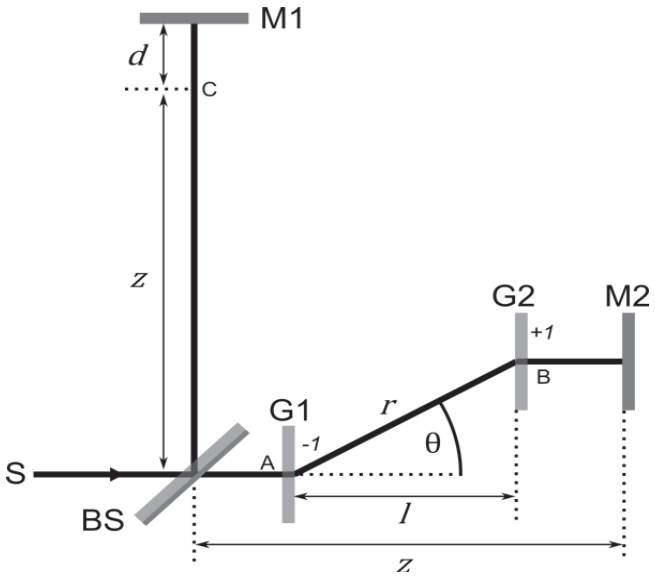

Figure 1 - Schematic representation of the interferometer.

The measurement arm is simply comprised of a measurement mirror (M1). When the position of M1 is such that the path from BS to M1 is the same as the perpendicular distance from the beam splitter to the reference mirror (M2) then the interferometer is said to be balanced and the optical path difference (OPD) between arms is zero. At this point, (C), the resulting interferogram (Figure 2) is centred on the spectrometer detector. As the distance of the measurement mirror moves from the balance point, C, a different wavelength comes into balance and so the point of symmetry of the interferogram moves across the detector. Post-processing of the interferogram allows this centre of symmetry to be calculated and thus the measurement mirror position inferred.

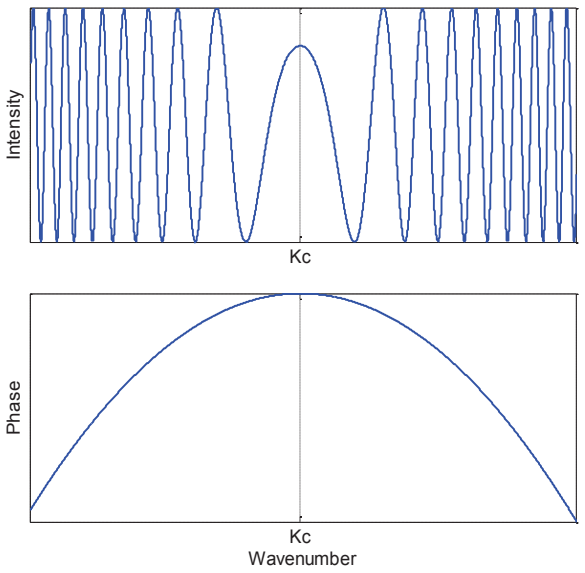

Figure 2 – Simulated phase difference (lower) and interferometer output intensity (upper) against angular wavenumber, k.

3. Experimental Apparatus

In the experimental apparatus shown in Figure 3 a narrow bandwidth (20 nm, centred on 829.2 nm) near infrared super luminescent diode (SLD) is used as a light source. It is linked by fibre to a collimator (FC) resulting in an output beam with a $1/e^2$ width of 8.3 mm. This beam is split by a beam splitter (BS) to form the measurement and reference arms.

In the reference arm a pair of matched transmission gratings (G1, G2) with a perpendicular separation of 330 mm is used. These 25 mm^2 gratings have a groove density of 300 lines/mm. The negative and positive diffracted first orders are taken from G1 and G2 respectively. All other diffracted orders are blocked. The reference mirror, M2, reflects the reference arm beam back through the grating pair to the beam splitter.

In the measurement arm a folding mirror M3 is used to redirect the beam on to the measurement mirror, M1, this is due to space constraints on the optics workbench. The measurement mirror is mounted on a high precision, closed loop piezo-electric translator (PZT), allowing precise control of the mirror position along the Z axis to enable the testing of range, resolution and linearity of the interferometer.

After recombination of the measurement and reference arm beams at the beam splitter, a spectrometer comprised of a reflective grating (G3), a spherical mirror (SM) and a CMOS line array (D) is used to capture the resulting interferogram. The line detector (ISG Lightwise LW-SLIS-2048A) is 2048 pixels wide with 12-bit resolution and a maximum line rate of 27 kHz.

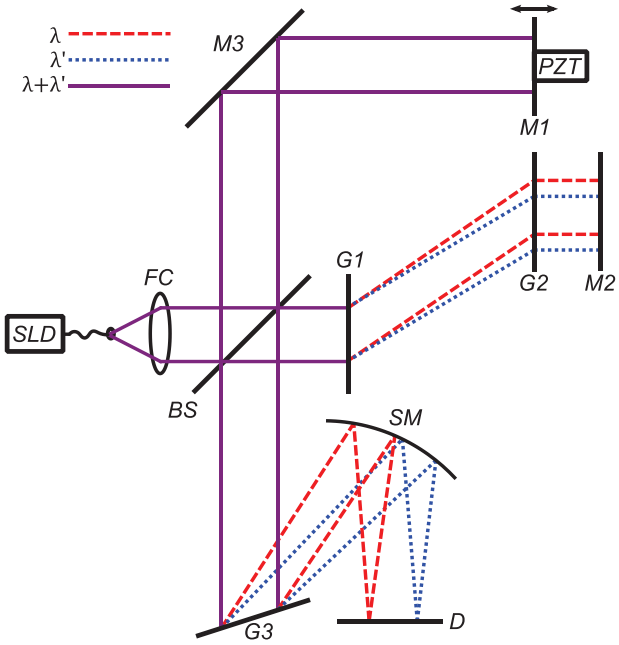

Figure 3 - Bulk optics experimental apparatus.

Finally, a custom Labview visual instrument processes the resulting interferogram to extract the balance point. An autoconvolution algorithm is applied to the interferogram, the pixel number of the highest point from this calculation is taken as the interferogram centre and hence the mirror or sample position. A transparent plastic enclosure was constructed to exclude dust and minimize environmental disturbances such as air flow and temperature variations.

4. Previous Results

Figure 4 shows an interferogram captured by the detector (red) as well as a computed autoconvolution result (blue).

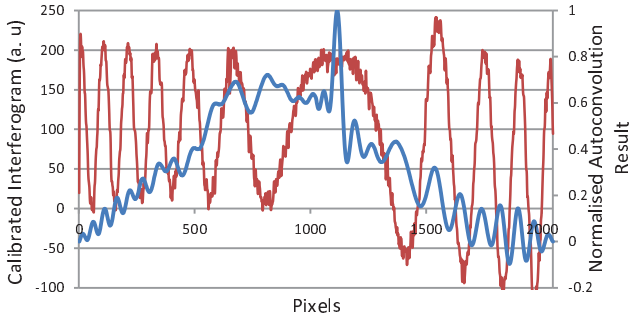

Figure 4 - A real interferogram (red) and convolution result (blue)

For the purpose of determining linearity, vertical resolution and range a closed-loop precision PZT (Physik Instrumente P-721.CLQ) was used. It uses a capacitive displacement sensor to achieve linearity of better than 0.03 % and a bi-directional repeatability of less than 5 nm over a working range of 100 µm.

The PZT may be stepped in small increments to change the distance of the measurement mirror, M1, from the

balance point, C. Figure 5 (a) shows the progression of the fringe centre detected by autoconvolution as the measurement mirror position is moved in 5 µm increments. Due to the limited range of the PZT the linearity was not tested across the entire DRI range. The graph in (b) shows deviation of (a) from a linear fit.

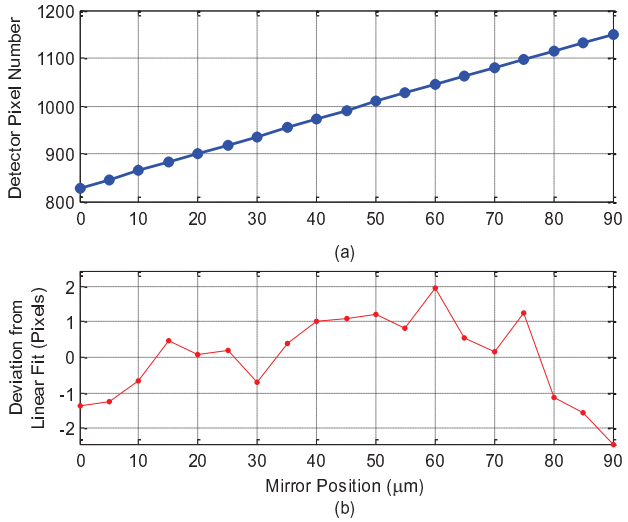

Figure 5 - (a) Recorded balance point as the measurement mirror is moved; (b) Deviation from a least squares linear fit.

A least squares linear fit to the plotted data has a gradient of 3.58 pixels/µm, providing a resolution of 279 nm. Over the full 2048 pixel range of the detector this gives a theoretical maximum range of 569 µm although in practice it is less than this (300 µm) since as the point of symmetry approaches either side of the detector the autoconvolution result deteriorates. The overall linearity of the scale was found to be 0.842 % over the measured 100 µm range.

Finally, the profiling capability of DRI was tested by scanning a precision step height specimen (Rubert 513, ISO 5436 Part 1:2000, type D) in front of the measurement arm with a Newport translation stage (MFA-CC). A low N.A. (0.1) lens was used to focus the beam on the sample, resulting in a beam spot size of approximately 6.5 µm.

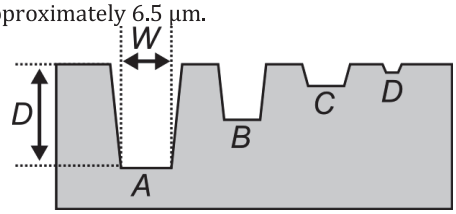

Figure 6 - Rubert step sample 513. Depth, D, for A = 1000 µm, B = 500 µm, C = 200 µm and D = 30 µm.

Figure 7 shows the raw data output from a scan across profiles B and C. Clearly visible are areas of erroneous data either side of the step heights. These are caused by the high slope angle leading from the top surface to the bottom of the step. The high angle and low NA of the lens means that less light is reflected back into the measurement arm and fringe visibility is significantly or completely reduced.

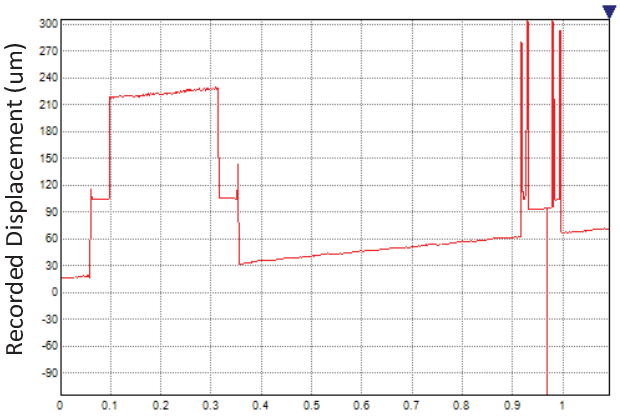

Figure 7 - Raw measurement data from profile across the 200 µm and 30 µm steps on the Rubert step sample.

Post-processing with a surface measurement analysis tool, Surfstand, eliminates these erroneous data points and inverts the data to better represent the sample (Figure 8). A measured step height of 199 µm was observed, with mechanical noise introduced by the translation stage thought to have caused the 1 µm difference as well as the oscillatory pattern in the middle of the trace. It is expected that these oscillations will be significantly reduced through an improved mechanical setup and calibration of the translation stage.

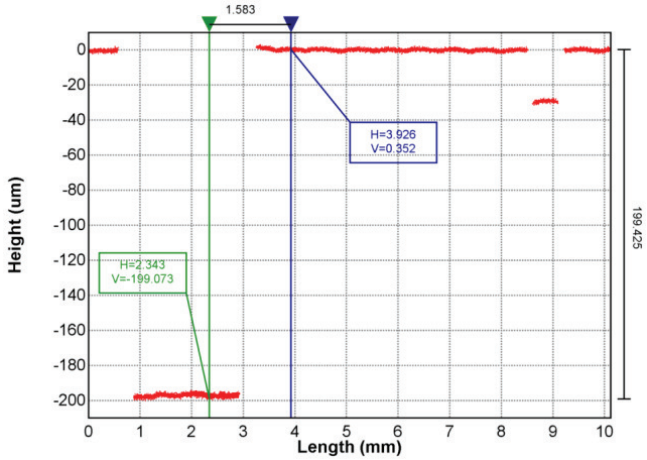

Figure 8 – Measured profile. Slope corrected and repaired step data.

5. High Resolution DRI

To achieve the desired high dynamic range it is necessary to improve the vertical resolution while maintaining the previously achieved range. A sub-nanometre vertical resolution DRI with the same or better range is therefore necessary.

The previous method uses autoconvolution to determine the point of interferogram symmetry and hence resolution is limited by the detector pixel size. When the

OPD is changed in large increments (microns), the interferogram centre moves across the CCD.

When smaller increments of OPD change are applied, the interferogram shape at the point of symmetry is seen to change. With these small changes (10s of nm or less) all of the interferogram maxima move outwards from the fringe centre until a new pair of maxima are formed. This leads us to consider a new method of higher resolution measurement using these interferogram maxima position changes. Figure 9 illustrates this behaviour; 40 nm increments in OPD were simulated with Matlab and the resulting fringe patterns plotted. This shape change continues as the OPD increases until the fringe shape wraps around to the first image (not shown).

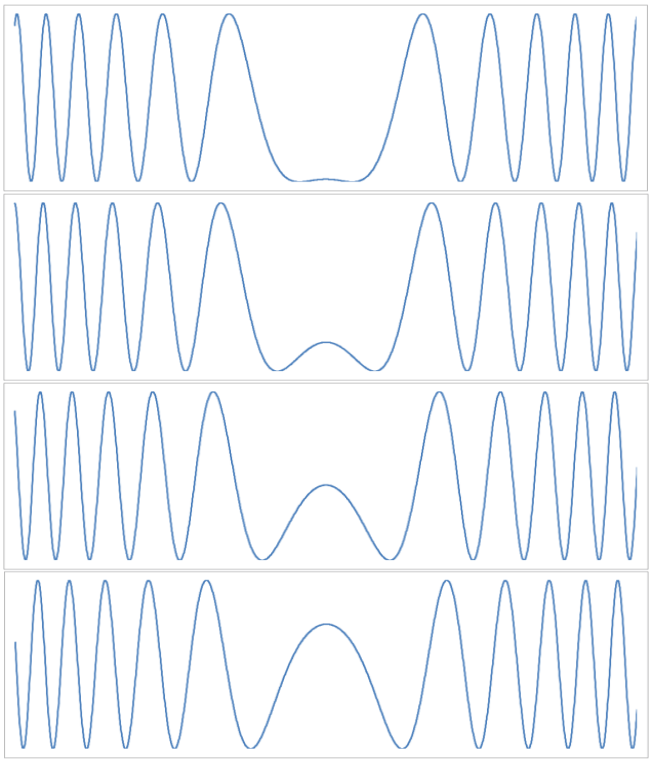

Figure 9 - Examples of fringe shape change as simulated OPD is increased from 0 to 120 nm in 40 nm increments. Only a small part of a ~400 nm cycle. X axis, pixel number. Y axis, intensity.

Knowing maxima position is altered by nanometre OPD changes, methods of extracting high resolution measurement data may be described by naming the fringe peaks to the left and right of the interferogram centre as negative and positive respectively. Figure 10 illustrates this peak/valley naming process. To find the position of these peaks a polynomial fit peak finding algorithm is used twice, once to find the peaks and once to find the valleys. Next, the autoconvolution algorithm is used to find the centre of the interferogram as per the previous method. The arrays of peaks and valleys are reindexed to reflect their position in relation to the fringe pattern centre.

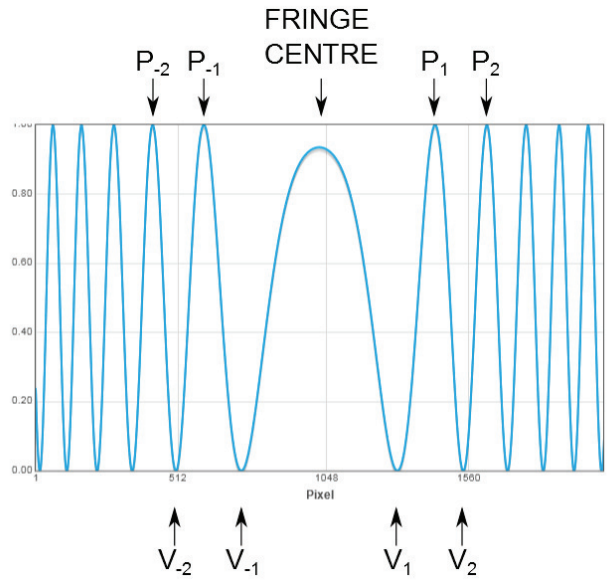

Figure 10 - Fringe peak labelling scheme applied to a simulated interferogram.

5.1. Single Peak Tracking

Figure 9 shows only four discrete steps of a continuous cycle. By simulating multiple interferograms with varying OPDs and plotting the position of P_1 for each, the cyclic nature of the peak position may be illustrated.

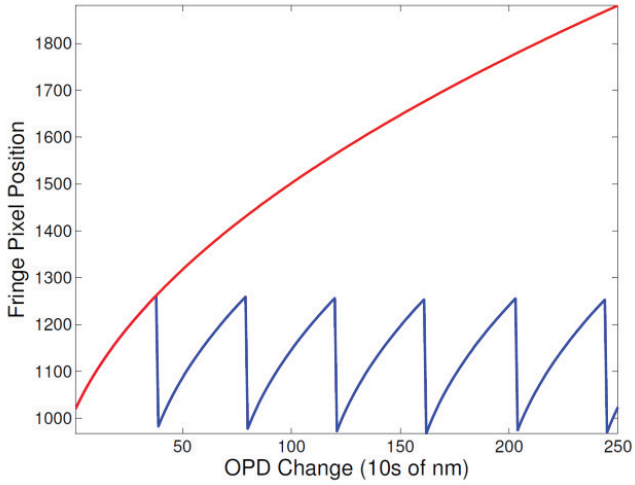

Figure 11 – Simulated P_1 position with OPD change (blue) and peak tracked as new ones form at the interferogram centre. A single peak tracked across the entire detector (red).

From Figure 11 it is apparent that the movement of a peak across the CCD is non-linear and cyclic, suggesting that a high resolution relative method is possible. The blue line shows the position of P_1 as the OPD is increased, approximately every 400 nm of OPD change a new peak is formed at the fringe centre and becomes the new P_1. The red line ignores the creation of new peaks at the centre and simply tracks the progress of a single peak across the CCD.

The problem with tracking a single peak is that as the OPD changes enough to influence the point of symmetry of the interferogram, the pixel at which the peak position

wraps around will change. This is illustrated by Figure 12 for which the simulated OPD was increased in 20 nm increments and the position of P_1 for each generated interferogram recorded.

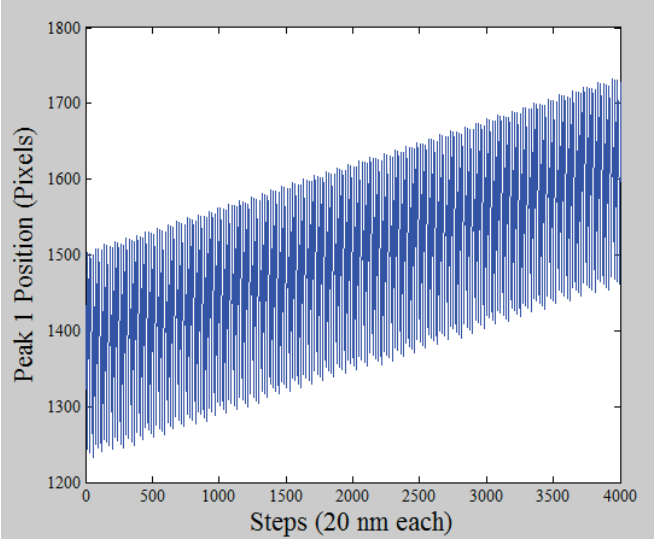

Figure 12 – Simulate position of P_1 as OPD is changed from 0 to 80 µm in 20 nm increments.

5.2. Peak Separation Tracking

A more robust method of finding high resolution data is hence required. The solution is to calculate the separation between P_1 and P_{-1}.

$$Peak\ Separation = P_1 - P_{-1}$$

This results in a value for the pixel position change for each cycle that is constant irrespective of the interferogram symmetry location on the CCD, effectively removing the slope seen in Figure 12.

This improved method is matched by measurements taken with the experimental bulk optics setup. The Physique Instruments PZT was used to move the measurement mirror in 2 nm increments while the peak (P_1-P_{-1}) and valley (V_1-V_{-1}) separation was recorded.

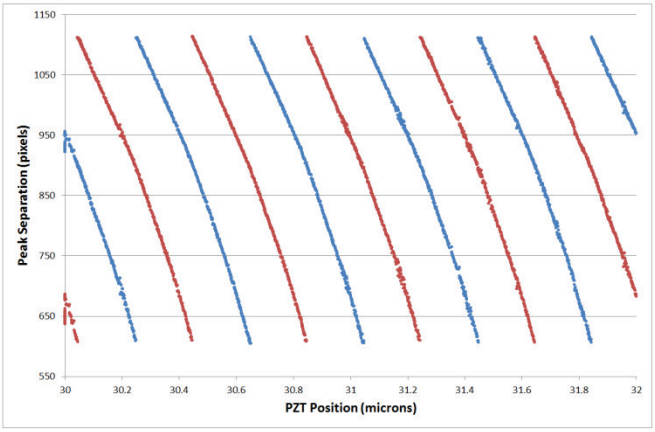

Figure 13 - Real DRI data. Peak (blue) and valley (red) separation across 2 µm as the OPD is incremented in 2 nm steps with a precision PZT.

In Figure 13 the curvature present in the simulations is visible and appears similar but the direction of curvature is inverted due to an inverted direction of measurement mirror movement.

From this simulated and real data we can begin to describe the behaviour of these peak movements. It is important to know the OPD change required to cause the peak separation to wrap around. This may then be used as a high resolution relative measurement method and the lower resolution but higher range absolute measurement provided by the autoconvolution method may be used to resolve the ambiguity of this new relative measurement method.

Using the data from Figure 13 the distance between wrap arounds was calculated by taking the average of four wrap arounds. This was repeated for the highest and lowest values for the peaks and for the valleys giving four values to compare.

Peaks	(31.840 - 30.244) / 4 =	**0.3990 µm**
	(31.844 - 30.250) / 4 =	**0.3985 µm**
Valleys	(31.640 - 30.040)/4 =	**0.4000 µm**
	(31.646 - 30.044) / 4 =	**0.4005 µm**

Table 1 – Calculated range for experimental high resolution DRI data.

This gives an approximate wraparound value and hence range of 400 nm. The noise independent vertical resolution of this method will depend upon the grating separation, d, and the spectrometer parameters since resolution is dependent on how far a peak moves across the CCD before a new one is formed. This increased resolution will come at the cost of usable range since with less peaks and valleys on the spectrometer the autoconvolution result will fail further from the CCD edge.

5.3. Effect of dispersion on resolution

The diagrams in Figure 14 illustrate the number of fringe peaks and valleys present at the CCD for a perpendicular grating separation, d, of 660 mm (top) and 115 mm (bottom) for simulations of a pair of 300 lines/mm gratings.

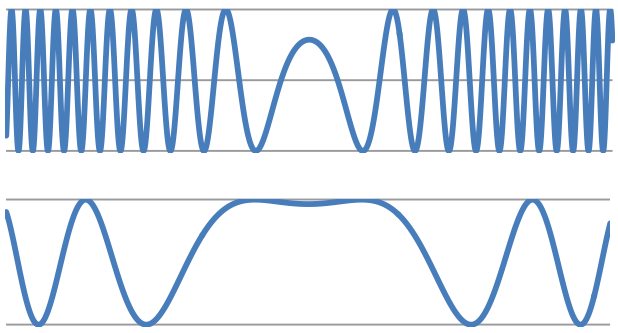

Figure 14 - Simulations of 660 mm grating spacing (top (a)) and 115 mm grating spacing (bottom (b)).

It is apparent from these graphs that the larger grating spacing (660 mm) has more peaks and so the peak position will move less pixels before new peaks are formed when compared to the smaller grating spacing (115 mm). This will result in a lower resolution.

A more important consideration when choosing the grating spacing is that the resolution of the autoconvolution method must be sufficient to resolve the ambiguity of the relative peak separation method. This is discussed in more detail in further work.

5.4. Effect of dispersion on range

A final consideration when investigating this method is which system properties affect the range. Use of Matlab for simulations confirmed that grating spacing has no effect on the approximate 400 nm range. It was found through similar simulations that source wavelength is the determining factor for the distance travelled before wraparound. The DRI setup uses a fibre linked 820 nm SLD from Exalos as the light source. When measured with an Optical Spectrum Analyser (OSA), the central wavelength is 828.85 nm with a bandwidth of 10.8 nm Using specifications for other SLDs available from the Exalos website, simulations were run to find the theoretical range for other available SLDs. The results of these may be found in Table 2 and prove that the range of high resolution DRI is half the central wavelength in each case. This closely matches the experimental results in Table 1, the slight difference is to be investigated in future work.

The confirmation of this allows future work to consider if a different SLD choice could yield increased efficiency or lower system cost, since the availability of the optical components required may change with wavelength range used.

Centre Wavelength (nm)	Bandwidth (nm)	Exalos Part Number	Result (nm)
650	10	EXS210035-02	325
750	20	EXS7505-8411	375
820	25	EXS210036-01	410
828.85	10.85	Above, OSA Measured	814
1050	60	EXS210063-01	524

Table 2 - Simulated range findings for a selection of SLDs available from Exalos.

6. Conclusions

A summary of previous dispersed reference interferometry has been presented and the importance of further signal processing to extract high resolution phase information highlighted.

A method to calculate high resolution phase information from existing interferograms was presented along with additional signal processing methods to improve linearity and characterise range and resolution. Finally a study of the effect of critical system parameters on the range and resolution of this method was evaluated.

7. Further Work

- Shortening of the grating spacing, d, to achieve a higher resolution with the autoconvolution method. A resolution of 130 nm will allow the phase ambiguity of the peak separation method described in this paper to be resolved and the two methods to be combined, achieving the desired high axial dynamic range required.
- Study of non-linear dispersion in the reference arm and the effect it has on interferogram peak tracking accuracy.
- Investigation of methods to increase measurement rate. These include improved dispersion efficiency, signal processing and use of FPGAs to pre-process data to achieve the target 10 KHz measurement rate.
- The recent availability of small (100 μm) and light commercially available fibre probes with novel side firing geometries will lead to the development of an unbalanced fibre based interferometer to allow use of these small fibre probes on-machine as well as in previously impossible or difficult to measure places.

8. Acknowledgements

The authors gratefully acknowledge the UK's Engineering and Physical Sciences Research Council (EPSRC) funding of the EPSRC Centre for Innovative Manufacturing in Advanced Metrology (Grant Ref: EP/I033424/1) and the European Research Council Surfund Project (ERC-228117).

9. References

Häusler, P. P. a. G. (2005). "White-light interferometer with dispersion: an accurate fiber-optic sensor for the measurement of distance." Applied Optics.

Martin, H. J., X; (2013). "Dispersed Reference Interferometry." CIRP Annals Manufacturing Technology.